NASA/TM—2017–218233

Analytical Round Robin for Elastic-Plastic Analysis of Surface Cracked Plates, Phase II Results

P.A. Allen and D.N. Wells
Marshall Space Flight Center, Huntsville, Alabama

March 2017

The NASA STI Program…in Profile

Since its founding, NASA has been dedicated to the advancement of aeronautics and space science. The NASA Scientific and Technical Information (STI) Program Office plays a key part in helping NASA maintain this important role.

The NASA STI Program Office is operated by Langley Research Center, the lead center for NASA's scientific and technical information. The NASA STI Program Office provides access to the NASA STI Database, the largest collection of aeronautical and space science STI in the world. The Program Office is also NASA's institutional mechanism for disseminating the results of its research and development activities. These results are published by NASA in the NASA STI Report Series, which includes the following report types:

- TECHNICAL PUBLICATION. Reports of completed research or a major significant phase of research that present the results of NASA programs and include extensive data or theoretical analysis. Includes compilations of significant scientific and technical data and information deemed to be of continuing reference value. NASA's counterpart of peer-reviewed formal professional papers but has less stringent limitations on manuscript length and extent of graphic presentations.

- TECHNICAL MEMORANDUM. Scientific and technical findings that are preliminary or of specialized interest, e.g., quick release reports, working papers, and bibliographies that contain minimal annotation. Does not contain extensive analysis.

- CONTRACTOR REPORT. Scientific and technical findings by NASA-sponsored contractors and grantees.

- CONFERENCE PUBLICATION. Collected papers from scientific and technical conferences, symposia, seminars, or other meetings sponsored or cosponsored by NASA.

- SPECIAL PUBLICATION. Scientific, technical, or historical information from NASA programs, projects, and mission, often concerned with subjects having substantial public interest.

- TECHNICAL TRANSLATION. English-language translations of foreign scientific and technical material pertinent to NASA's mission.

Specialized services that complement the STI Program Office's diverse offerings include creating custom thesauri, building customized databases, organizing and publishing research results…even providing videos.

For more information about the NASA STI Program Office, see the following:

- Access the NASA STI program home page at <http://www.sti.nasa.gov>

- E-mail your question via the Internet to <help@sti.nasa.gov>

- Phone the NASA STI Help Desk at 757–864–9658

- Write to:
  NASA STI Information Desk
  Mail Stop 148
  NASA Langley Research Center
  Hampton, VA 23681–2199, USA

NASA/TM—2017–218233

Analytical Round Robin for Elastic-Plastic Analysis of Surface Cracked Plates, Phase II Results

P.A. Allen and D.N. Wells
Marshall Space Flight Center, Huntsville, Alabama

National Aeronautics and
Space Administration

Marshall Space Flight Center • Huntsville, Alabama 35812

March 2017

Acknowledgments

The authors would like to acknowledge the support of the ASTM Committee on Fatigue and Fracture (E08). Clearly, the most important part of any round robin study is the group of participants graciously lending their time and effort to the undertaking. We would like to sincerely thank each of them: Steven Altstadt at Stress Engineering Services, Jason Bely at Alcoa, Enrico Lucon at the National Institute of Standards and Technology, Francisco Martin and Ryan Sherman at Purdue University, Dawn Phillips at NASA Marshall Space Flight Center, Greg Thorwald at Quest Integrity Group, Igor Varfolomeev at the *Fraunhofer-Institut fuer Werkstoffmechanik IWM* (Germany), and Michael Windisch at MT Aerospace AG (Germany). We greatly appreciate their efforts in helping us move the surface crack test standard forward.

Available from:

NASA STI Information Desk
Mail Stop 148
NASA Langley Research Center
Hampton, VA 23681–2199, USA
757–864–9658

This report is also available in electronic form at
<http://www.sti.nasa.gov>

TABLE OF CONTENTS

LIST OF FIGURES

LIST OF FIGURES (Continued)

LIST OF TABLES

LIST OF ACRONYMS

API	American Petroleum Institute
ASTM	American Society for Testing and Materials
CMOD	crack mouth opening displacement
EPFM	elastic-plastic fracture mechanics
FEA	finite element analysis/analyses
FEM	finite element modeling
ILS	interlaboratory study
LEFM	linear-elastic fracture mechanics
SDAR	slope determination by analysis of residuals
TASC	Tool for Analysis of Surface Cracks (software)
TM	Technical Memorandum

NOMENCLATURE

ℓ	crack extension
$2c$	total surface crack length
a	surface crack depth
B	plate thickness
C	deformation limits
CMOD	crack mouth opening displacement
CMOD_i	crack mouth opening displacement at crack tearing initiation
c	half-crack surface length
E	elastic modulus
J	J-integral
J_p	peak J-integral
K	stress intensity factor
K_ϕ	stress intensity factor at ϕ_i
N	notch height
n	strain hardening exponent
P_i	test force at crack tearing initiation
Q	difference between constraint-influenced opening mode stress and a reference stress field parameter
r	radial distance from crack
$r_{\phi a}$	characteristic length of specimen
$r_{\phi b}$	characteristic length of specimen

NOMENCLATURE (Continued)

T	T-series, linear-elastic constraint state
α_h	constraint parameter
ϕ	parametric angle
ϕ_i	initiation angle
ν	Poisson's ratio
σ	stress
σ_{ys}	yield stress
σ_{yy}	opening mode stress

TECHNICAL MEMORANDUM

ANALYTICAL ROUND ROBIN FOR ELASTIC-PLASTIC ANALYSIS OF SURFACE CRACKED PLATES, PHASE II RESULTS

1. INTRODUCTION

The ASTM Committee on Fatigue and Fracture (E08) Task Group on Fracture Toughness of Surface Cracks (E08.07.03) has developed a new material test standard for the assessment of surface crack toughness in the linear-elastic and the elastic-plastic regime, E2899.[1] While evaluation of the linear-elastic stress intensity factor, *K*, is well-accepted for surface crack geometries through the Newman-Raju equations[2,3] or other existing tabulations,[4] the evaluation of elastic-plastic *J*-integral values requires the user to perform an analysis of the experiment using methods that cannot be easily contained or conveyed within a test standard. The feasibility of allowing this latitude in assessment methodology in a testing standard requires validation through an interlaboratory study (ILS). This Technical Memorandum (TM) provides an overview of the problem statement and results of the second phase of the study.

1.1 Motivation for the Interlaboratory Study

Existing mechanical testing standards for fracture mechanics applications, such as ASTM E1820,[5] include within the document all the necessary equations and supporting data to assess the experiment directly, producing a 'standard' result. In the case of a surface crack in a flat plate, no openly available method exists for accurately evaluating the *J*-integral under elastic-plastic conditions along the full perimeter of a surface crack that can feasibly be reduced to equation form for inclusion into a test standard. However, the ability to assess this problem using methods of analysis such as finite elements has progressed considerably in recent years and may now be a suitable substitute for assessment of experimental results in lieu of equations defined within the standard. Codes defining standard practice for structural evaluation of defects, such as the API Recommended Practice for Fitness for Service,[4] allow for such external analysis methods. This study is designed to evaluate the variability in the use of an external analysis method for experimental data assessment.

1.2 Scope and Objectives for the Interlaboratory Study

This ILS is planned for development in phases based on need and observations made as the study progresses. Additional phases are likely to investigate different crack shapes, bending as opposed to tension loading, and different materials. This work was conducted under the auspices of ASTM ILS 732. The first phase of the ILS is documented in NASA/TM—2012–217456,[6] and approached the ILS concept differently than most experimentally based studies. The analysis

methodology was not specified to participants and key experimental results were withheld. This made phase I of the study 'blind' in the sense that the participants did not have the experimental force and displacement information available to them to validate their model, or to potentially alter their model to converge on the experimental result, and they were free to approach the analysis using any method of choice. This approach allowed this first phase of the ILS to serve as a current measure of the state of the art for elastic-plastic fracture mechanics analysis. An open study of this nature regarding elastic-plastic analysis methods had not been performed for some time.[7,8] Examination of the phase I results, as detailed in reference 6, isolated the sources of variability in the finite element analysis (FEA) and identified the common analytical practices. These findings led to the contents of Annex A6 in E2899, "Methodology for performing elastic-plastic finite element analysis and comparison with test record."

The objective of phase II is to enhance the findings from phase I of this activity by continuing to collect independent analysis of surface cracks in tension by requesting participants perform an FEA of a new experiment while adhering to the methodology of the E2899 Annex A6 as closely as possible. The expectation being that, if each participant's analysis follows the best practices defined by Annex A6, the variability in results would be reduced relative to the (already favorable) observations in phase I. This second phase also differs significantly from the first phase in that the full experimental test records are provided to the participants. In addition to the FEA, the study participants were asked to interpret the test results according to E2899. This involves evaluating crack-front constraint, determining a critical initiation angle (ϕ_i) along the crack front, determining the deformation regime of the test (linear-elastic fracture mechanics (LEFM), elastic-plastic fracture mechanics (EPFM), or field collapse), and determining the critical J-integral value. The intent was that this process would familiarize participants with the standard and provide the task group with helpful feedback regarding the clarity of the language in the written requirements of the standard.

In addition to the FEA of the test, the task group is interested in evaluating a potential new means of analysis of surface crack experiments suitable to the standard. Allen[9,10] has developed an interpolation tool to evaluate surface cracks in tension across a wide range of semi-elliptical crack aspect ratios and material behavior. The interpolation tool works with a broad database of 600 solutions of surface cracks under a deformation state extending to the limits of the elastic-plastic regime. The software that interpolates this space, Tool for Analysis of Surface Cracks (TASC), is available free of charge.[11] For participants willing and able to perform FEA but also interested in TASC, the authors requested that the FEA work be completed prior to assessing the test with TASC. For those interested in evaluating the test but unable to participate in the FEA work, study participants were also allowed to evaluate the problem using only TASC.

The experimental test for this second phase of the ILS was planned as a ductile tearing test on steel with moderate yield strength providing a result well into the EPFM regime, beyond the limits of LEFM validity. The choice of readily available 4142 steel proved inappropriate when unstable cleavage failure occurred—it had not occurred to us that the transition temperature for 4142 may be as high as 100 °C. Our intent was to produce a fracture surface with an identifiable location of maximum stable ductile tearing along the crack front so participants could identify the critical initiation angle from an image of the fracture surface. This would provide insight into the repeatability of this required image measurement. In this case, though the test did reveal some

stable tearing, the fracture surface did not provide obvious evidence in the ductile tearing of the initiation angle for test evaluation. Instead, participants were requested to work through the process described in E2899 Annex A5 to identify the initiation angle by using the product of the *J*-integral and constraint (*T*-stress). For this ILS activity, the authors chose to proceed with an assessment of this test because it fully suits the purpose, in spite of section 1.8 of E2899 which declares cleavage results being outside of the scope of the standard.

2. PROBLEM STATEMENT

The participants were asked to evaluate a surface crack tension test according to the version of the standard published at that time, E2899-13. The basic geometry and definition of parameters for a generic surface crack specimen are shown in figure 1. The complete problem statement as it was provided to each participant is included as appendix A. A compressed archive file was provided to each participant containing the following data: instructions, material identification, and uniaxial tension stress and strain data, force versus crack mouth opening displacement (CMOD) record for the surface crack tension test, and the surface crack fracture surface photo with basic crack size measurements. These data represent the fundamental information provided by a mechanical test laboratory prior to evaluating the test result. The choice of FEA constitutive models and treatment of the stress-strain data was left to the discretion of the participants.

From their evaluation of the test per E2899, each participant was requested to provide several results including the fracture toughness test result in K or J at the critical initiation angle (ϕ_i), crack front constraint quantification in terms of T-stress, and interpretation of selected validity criteria. Spreadsheets for recording analysis results were provided to enhance consistency in reporting and to clarify what data were being requested. See appendix A for details.

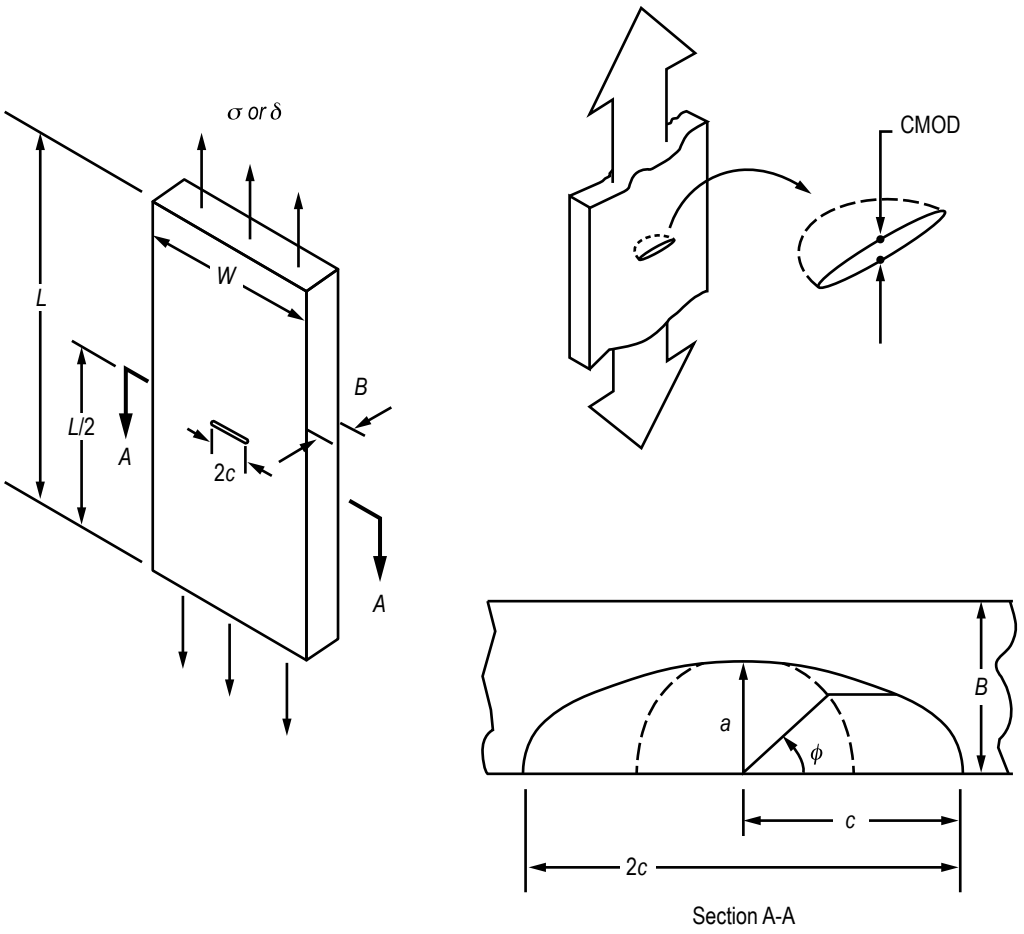

Figure 1. Surface crack test specimen configuration.

3. PARTICIPANT OVERVIEW

This phase of the study had 10 participants covering a range of industries, academia, and nationalities. There was also intent to include participants with a broad range of expertise in the study. The user community for the test standard is potentially broad; therefore, our intent was not to have only 'experts' in the field participating. A study with only expert participants would not be properly representative, leading to overly optimistic results and a lack of proper feedback on the test standard.

A list of the participants is included in table 1. All participants have been assigned a random designation from Lab-1 to Lab-10, with Lab-1 representing the authors' results. All results remain anonymous, though each participant was informed of their lab identification.

Table 1. ILS participants and affiliation.

Name	Affiliation
Phillip Allen	MSFC Materials Laboratory
Steven Altstadt	Stress Engineering Services
Jason Bely	Alcoa
Enrico Lucon	National Institute of Standards and Technology
Francisco Martin	Purdue University
Dawn Phillips	MSFC Vehicle Structures
Ryan Sherman	Purdue University
Greg Thorwald	Quest Integrity Group
Igor Varfolomeev	*Fraunhofer-Institut fuer Werkstoffmechanik IWM, Germany*
Michael Windisch	MT Aerospace AG, Germany

4. RESULTS AND DISCUSSION

The phase II experiment consisted of a 4142 steel surface crack tension specimen of the dimensions shown in appendix A. A photograph of the specimen during test (fig. 2) shows the ring gauge used for CMOD measurement. The specimen was precracked in tension, instrumented, and then loaded monotonically while monitoring the force and CMOD values. The test intent was to load the specimen to an estimated critical CMOD value for the initiation of ductile tearing and then unload and fatigue marker-band the specimen to highlight any region of crack tearing. But, as mentioned earlier, the specimen failed in an unstable fashion due to cleavage before the estimated critical CMOD was reached. After consideration, the decision was to not repeat the test but to proceed with this result for the ILS.

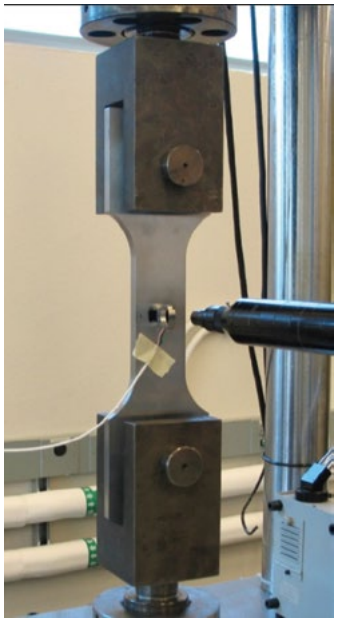

Figure 2. ILS specimen configured for testing.

The fracture surface for the ILS test (fig. 3) shows a largely uniform ductile crack extension (ℓ) of approximately 0.25 mm. Note that the cleavage initiation site can be identified, but this was not mentioned to the ILS participants. The minimum precrack extension was 1.30 mm and the electrical discharge machined initial notch height, N, was 0.43 mm. The CMOD value at specimen failure was 0.196 mm corresponding to a failure force of 603.5 kN. This information, combined with the force-CMOD response, constitute the experimental test result.

Figure 3. ILS specimen fracture surface.

4.1 Tying Analysis to Experiment

For a test result that falls outside the LEFM regime, the only physical tie between the test analysis and experiment is the force versus CMOD response. Based on this metric, E2899 requires agreement between the analysis and the experiment in two ways:—the slope of the force-CMOD elastic response and the final analytical force-CMOD prediction.

The force-CMOD response from the experiment is shown in figure 4. The nonlinearity in the test record is an indicator of elastic-plastic conditions in the specimen, and no unloading slope is plotted since the specimen exhibited unstable fracture. The force-CMOD predictions from the 10 ILS labs are plotted along with the experimental record in figure 5. Note that since some labs performed the analysis using both FEA and TASC, there is a total of 12 predictions, and the TASC results are designated by a '–*T*' suffix to the lab designation in the legend. The analytical predictions of the force-CMOD response show good overall agreement. Specific evaluations of the force-CMOD predictions in the linear region and at the failure CMOD of the test are discussed separately.

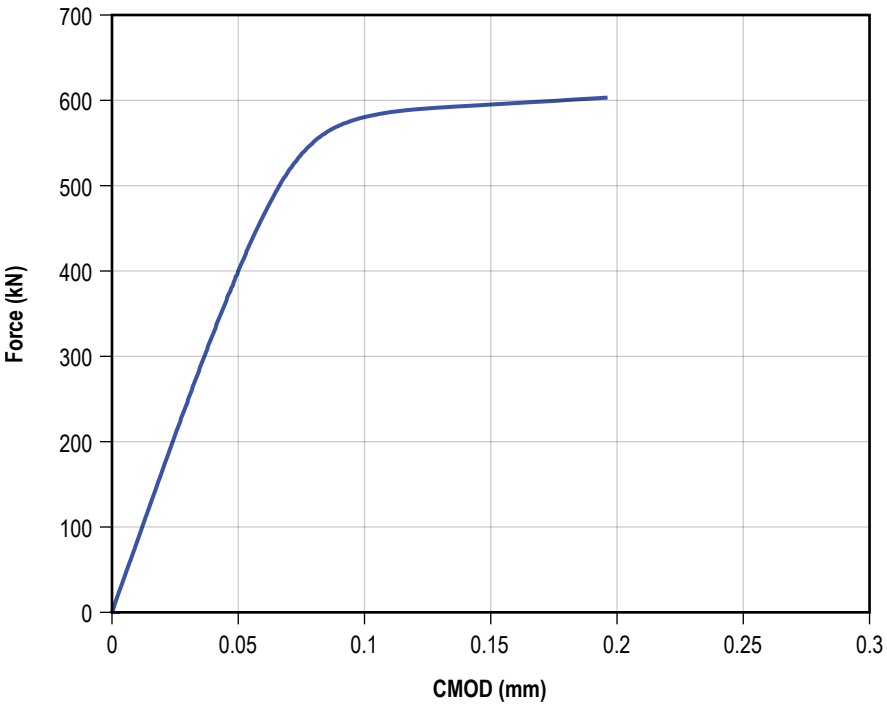

Figure 4. Experimental force versus CMOD response.

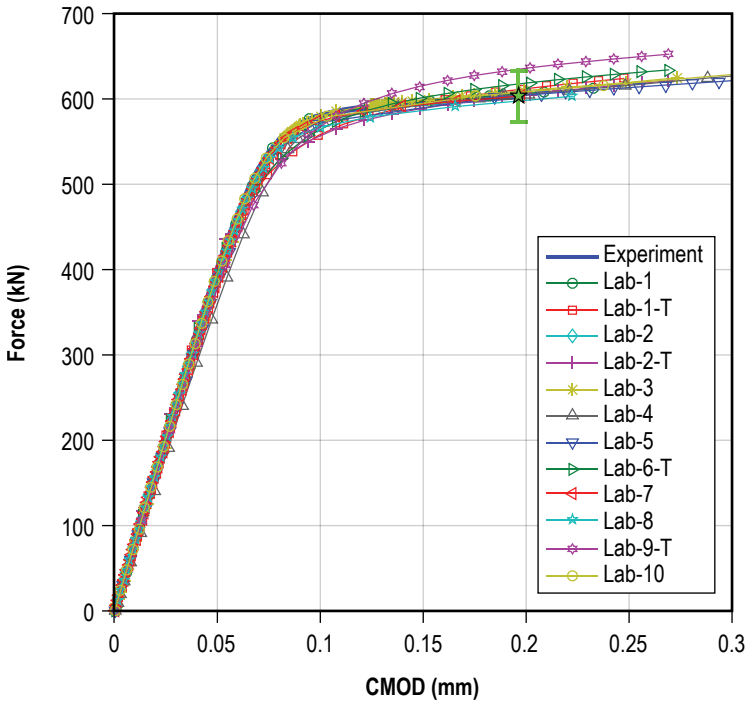

Figure 5. Force versus CMOD response for all ILS participants.

E2899 does not specify a procedure to determine the slope of the linear portion of the experimental force-CMOD response, so the slope of the linear portion of the test response was estimated using two methods: (1) Linear regression of the force-CMOD data falling within a fixed range of 20%–50% of the maximum force, and (2) the slope determination by analysis of residuals (SDAR) method as developed by Graham and Adler.[12] The elastic slope of each analysis result was determined using the first two load steps in the analysis where the material response is predominantly linear. The linear regression slope over the fixed range was 8,112 kN/mm and the SDAR slope was 8,291 kN/mm, for a difference of 2.2%. This reflects the long-standing concern regarding the challenge of accurately determining the slope of experimental records. The percent difference between the determined elastic slopes of the experiment and each analysis is presented in table 2. For the fixed range slope, all analytical predictions were within ±5% except for Lab-2-T and Lab-4. Using the SDAR method, all analytical predictions were within ±5% except for Lab-4 and Lab-9-T. For reference, Annex A6.3 of the E2899-13 version used by the ILS participants specified that "the most linear portion of the force-CMOD test record and elastic compliance of the finite element analysis result shall match within ±2.5%." Using this metric, only about half of the participants would have met the requirements for a valid analysis result, but, as will be shown later, the *J*-integral results between the labs are still in close agreement. The elastic compliance check in E2899 is intended to serve as a broad check on numerous basic inputs to the analysis such as specimen and crack geometry, material elastic properties, and boundary conditions to screen out fundamental analysis mistakes, but was not intended to be so stringent as to preclude otherwise acceptable analysis results. After studying the results of this ILS and considering the expected accuracy of slope determination from the experimental record, an elastic slope matching the requirement of ±5% was a more reasonable metric to meet the intent of the elastic compliance check. This change was implemented in the E2899-15 release of the test standard.

Table 2. Summary of elastic compliance evaluation results.

Experiment Elastic Slope Determined Using Linear Fit to 20%–50% of Max Data Range		Experiment Elastic Slope Determined Using SDAR Graham-Adler Fitting Algorithm	
Lab	**Elastic Slope % Diff.**	**Lab**	**Elastic Slope % Diff.**
Lab-1	0.06	Lab-1	2.23
Lab-1-T	–2.88	Lab-1-T	–0.66
Lab-2	–0.69	Lab-2	1.49
Lab-2-T	–5.55	Lab-2-T	–3.27
Lab-3	2.16	Lab-3	4.28
Lab-4	9.27	Lab-4	11.23
Lab-5	2.33	Lab-5	4.44
Lab-6-T	–2.47	Lab-6-T	–0.25
Lab-7	1.49	Lab-7	3.62
Lab-8	–0.63	Lab-8	1.55
Lab-9-T	3.30	Lab-9-T	5.39
Lab-10	–1.07	Lab-10	1.11

The second metric needed to correlate the analysis to the experimental result involves the values of force and CMOD recorded at the initiation of crack tearing, or, as in the case of this test result, at the point of unstable fracture. Since it is unlikely the test and analysis records will match exactly, an analyst must choose to evaluate the test result based on the analysis matching either the test initiation force, P_i, or the test initiation CMOD, CMOD_i. Though force is an intuitive descriptor of the test failure point, for elastic-plastic analysis, the CMOD is a more reliable predictor of the *J*-integral, because *J* is nearly a linear function of CMOD in the plastic regime.[6,10,13,14] E2899 specifies that the user determine the analysis reaction force corresponding to an analytical CMOD equal to CMOD_i from the experiment. For an analysis result to be considered valid, the analysis reaction force corresponding to CMOD_i shall be within ±5% of the experimental P_i. The green star symbol and error bar in figure 5 illustrates the test evaluation point and the ±5% force error band for this experiment. All of the ILS analytical force results corresponding to CMOD_i easily fall within the ±5% force error band except for Lab-9-T. The Lab-9-T force value exceeds P_i by 5.25%, but, since the results are just outside the chosen bounds, the Lab-9-T results are still included in the ILS.

4.2 Fracture Mechanics Analysis Results

To begin an analysis of a surface crack test, section 9.2 of E2899 requires users to determine the deformation regime of the test: linear-elastic, elastic-plastic, or field collapse regime. Determining the deformation regime is fundamental because each regime requires different treatment of the data for valid results calculation and reporting. Per E2899, for a test to be in the linear-elastic regime, the net section stress calculated using P_i must be less than 90% of the yield stress, σ_{ys}, and $r_{\phi a}, r_{\phi b} \geq C_K \left(J_K / \sigma_{ys} \right)$, where

$$J_K = \frac{\left(K_\phi \right)^2 \left(1 - \nu^2 \right)}{E} \tag{1}$$

and

$$C_K = \frac{E}{\sigma_{ys}}, \tag{2}$$

where

K_ϕ = linear elastic stress intensity factor calculated using P_i at the initiation angle, ϕ_i
ν = Poisson's ratio
$r_{\phi a}$ and $r_{\phi b}$ = characteristic lengths of the specimen test section at ϕ_i.

Figure 6 illustrates the definition of these characteristic lengths. Considering a 2D slice through the specimen along a path defined by $r_{\phi a}$ and $r_{\phi b}$, then $r_{\phi a}$ is analogous to a crack length measurement and $r_{\phi b}$ relates to a remaining ligament measurement. For the ILS phase 2 test, all of the participants correctly determined that both linear-elastic validity criteria were violated and, therefore, an elastic-plastic fracture mechanics analysis of the test must be performed.

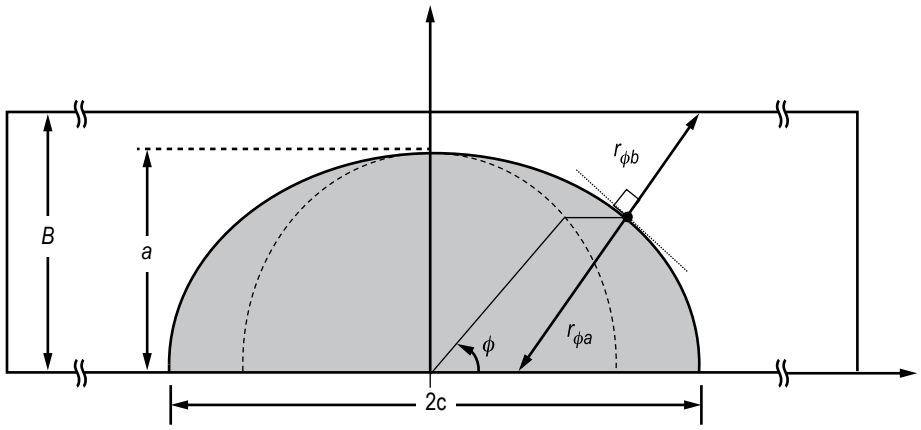

Figure 6. Cross section through the crack plane illustrating the characteristic lengths $r_{\phi a}$ and $r_{\phi b}$.

It is interesting to note that a test such as this, where ϕ_i is not clearly identifiable in the fracture surface, leaves the user in a bit of a conundrum. The user needs to know ϕ_i to be able to calculate K_ϕ, $r_{\phi a}$, and $r_{\phi b}$, but as described in Annex A5.2 of E2899, an elastic-plastic analysis is required to determine ϕ_i. In practice, a user can quickly perform the linear-elastic net section stress check, and if it is violated, move on to the more complicated elastic-plastic analysis step.

The as-reported J-integral versus ϕ results at CMOD_i from all ILS participants is shown in figure 7, where ϕ follows the common convention as defined in figure 1, with $\phi = 0$ at the free surface and $\phi = 90$ at the centerline crack depth location. Recall that, for this test, CMOD_i occurred at the point of unstable fracture and is therefore defined as the maximum CMOD measured prior to failure. In the initial review of the analysis results, the clear outlier was that the as-reported Lab-8 J-integral results were approximately one-half of the other participant's results. The Lab-8 reporting error is a common mistake in finite element domain integral calculations wherein the user forgets to double the finite element domain integral output due to the symmetry plane on the domain boundary. Once confirmed as the error, the Lab-8 J-integral results are included, thus they have been properly doubled for all reported values in this TM. This instance illustrates the value of an ILS exercise to highlight common mistakes so they can be addressed and prevented. Even after correcting the Lab-8 results by doubling them, it was observed that the Lab-8 results along with the Lab-5 results do not agree with the rest of the participant's results. With some investigation, it was discovered that the J values reported by Lab-8 and Lab-5 correspond to the analysis step where the FEA reaction force equals P_i instead of reporting J values at the FEA step corresponding to an analytical CMOD equal to CMOD_i as required in E2899. By anchoring their analysis result on force rather than CMOD, Lab-5 and Lab-8 reported their results at CMOD values smaller and larger than CMOD_i, respectively, resulting in J-integral distributions below and above the rest of the result family. With the data provided by Lab-5 and Lab-8, it was not possible for us to determine J-integral values corresponding to CMOD_i for each ϕ location from their results; therefore, a final consistent J-integral versus ϕ result at CMOD_i without Lab-5 and Lab-8 values are shown in figure 8. The overall shape of the J-integral distribution and range of J-integral values are a close match for most of the participants. Lab-4's result has a different behavior at $\phi = 0$, likely due to numerical free surface effects, and underestimates the increase in J values in the $15° \le \phi \le 45°$ range.

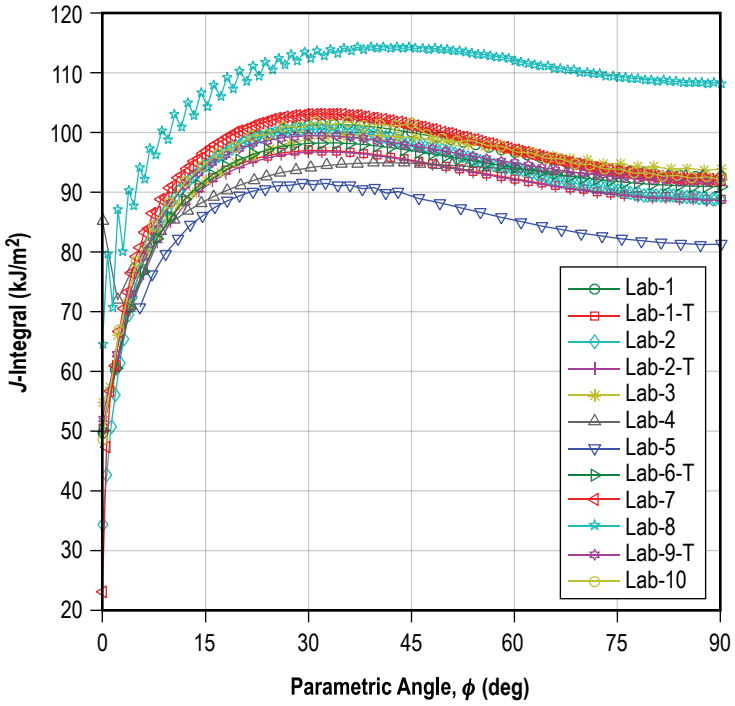

Figure 7. *J*-integral versus ϕ at the critical CMOD as reported by all participants.

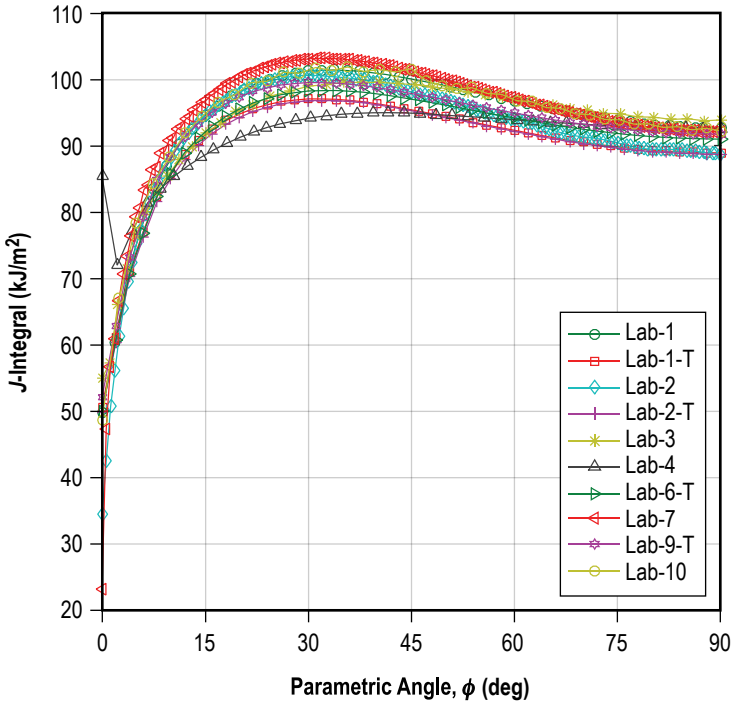

Figure 8. *J*-integral versus ϕ at the critical CMOD.

The next step in the fracture mechanics assessment of the test is the estimation of the critical initiation angle. As mentioned before, since ϕ_i could not be visually determined from ductile tearing evidence on the fracture surface, E2988 directed ILS participants to Annex A5 for the ϕ_i estimation methodology. Technical background information on the development and use of the E2988 Annex A5 methodology for ϕ_i estimation is given in appendix B. The following provides a brief summary. If ϕ_i cannot be determined from the fracture surface, Annex A5 directs the user to estimate ϕ_i by finding the value of ϕ which maximizes $f(\phi)$:

$$f(\phi) = \frac{J(\phi)}{J_p}\left(\frac{T(\phi)}{\sigma_{ys}} + 1\right) \text{ for } \frac{T(\phi)}{\sigma_{ys}} \leq 0$$

$$f(\phi) = \frac{J(\phi)}{J_p}\left(\frac{T(\phi)}{4\sigma_{ys}} + 1\right) \text{ for } \frac{T(\phi)}{\sigma_{ys}} > 0\,, \tag{3}$$

where

$J(\phi)$ = J-integral as a function of ϕ
J_p = peak J-integral value for all ϕ
$T(\phi)/\sigma_{ys}$ = T-stress as a function of ϕ normalized by the yield stress (tables are given in E2899 Annex A2).

Numerous previous studies have shown that, in most cases, initiation under uniform tension stress does not occur at the maximum value of the J-integral along the crack perimeter location, implying that the crack front constraint conditions are influencing the angle of initiation.[15–18] Therefore, equation (3) estimates the crack front location where the driving force and constraint combine to provide the highest likelihood for crack extension, based on the value of ϕ that maximizes their product. Figure 9 reproduces figure A5.2 from E2899 illustrating the methodology for the ϕ_i estimation using equation (3) (labeled as equation (A5.2) in the figure).

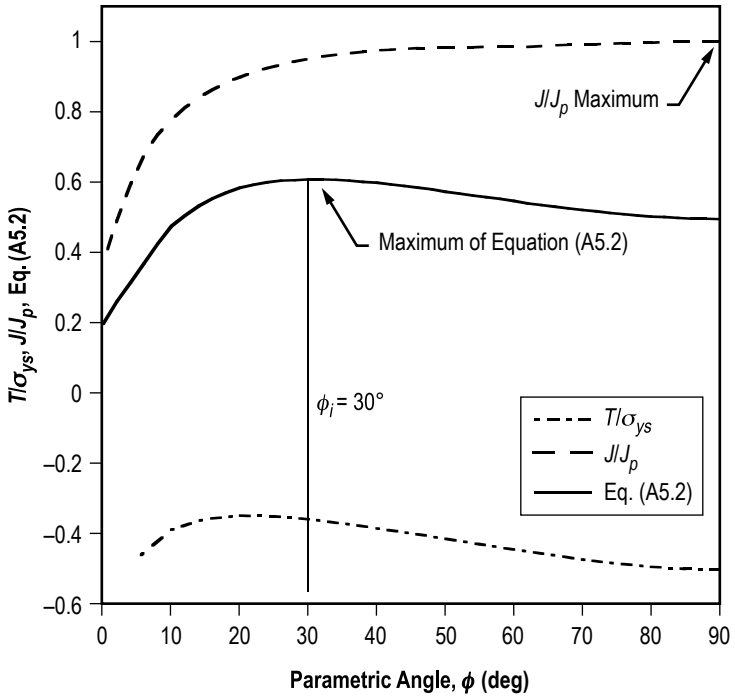

Figure 9. Figure A5.2 from ASTM E2899 illustrating the critical angle evaluation.

The calculated ϕ_i for all of the ILS participants is given in table 3a. Lab-10 had an error in their T-stress calculation which resulted in an incorrect ϕ_i value of 25° as reported. Using the correct T-stress, the corrected Lab-10 ϕ_i value is 35° which falls in line with the average of the results from all participants as shown in table 3b. Even including the Lab-10 results, the critical angle calculation results are very consistent with less than a 5° standard deviation in the result. Figure 10 shows the ILS results plotted on a sketch of the crack geometry with the predicted values shown by red markers on the crack front perimeter. Due to symmetry, only the $0° \le \phi \le 90°$ results are plotted but another set of critical angles exist and could be plotted in the left-hand quadrant as well. Figure 11 shows the same ϕ_i predictions plotted on the fracture surface of the ILS specimen. It is noteworthy that, to the trained eye, the cleavage river patterns on this fracture surface point back to the predicted initiation location, which serves as another affirming validation of the methodology.

Table 3a. Summary of critical angle evaluation results.

Lab	ϕ_i (deg)
Lab-1	37.5
Lab-1-T	36.0
Lab-2	35.0
Lab-2-T	36.0
Lab-3	40.4
Lab-4	37.1
Lab-5	36.0
Lab-6-T	38.0
Lab-7	34.9
Lab-8	42.8
Lab-9-T	30.0
Lab-10	25.0

Max.	42.8
Avg.	35.7
Min.	25.0
Std. Dev.	4.6

Table 3b. Summary of critical angle evaluation results with corrected T-stress for Lab-10.

Lab	ϕ_i (deg)
Lab-1	37.5
Lab-1-T	36.0
Lab-2	35.0
Lab-2-T	36.0
Lab-3	40.4
Lab-4	37.1
Lab-5	36.0
Lab-6-T	38.0
Lab-7	34.9
Lab-8	42.8
Lab-9-T	30.0
Lab-10	35.0

Max.	42.8
Avg.	36.6
Min.	30.0
Std. Dev.	3.1

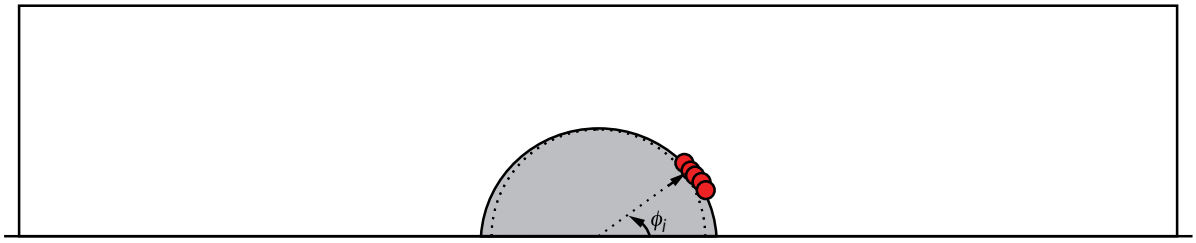

Figure 10. Illustration of the critical angle values for all ILS participants plotted on a sketch of the crack front.

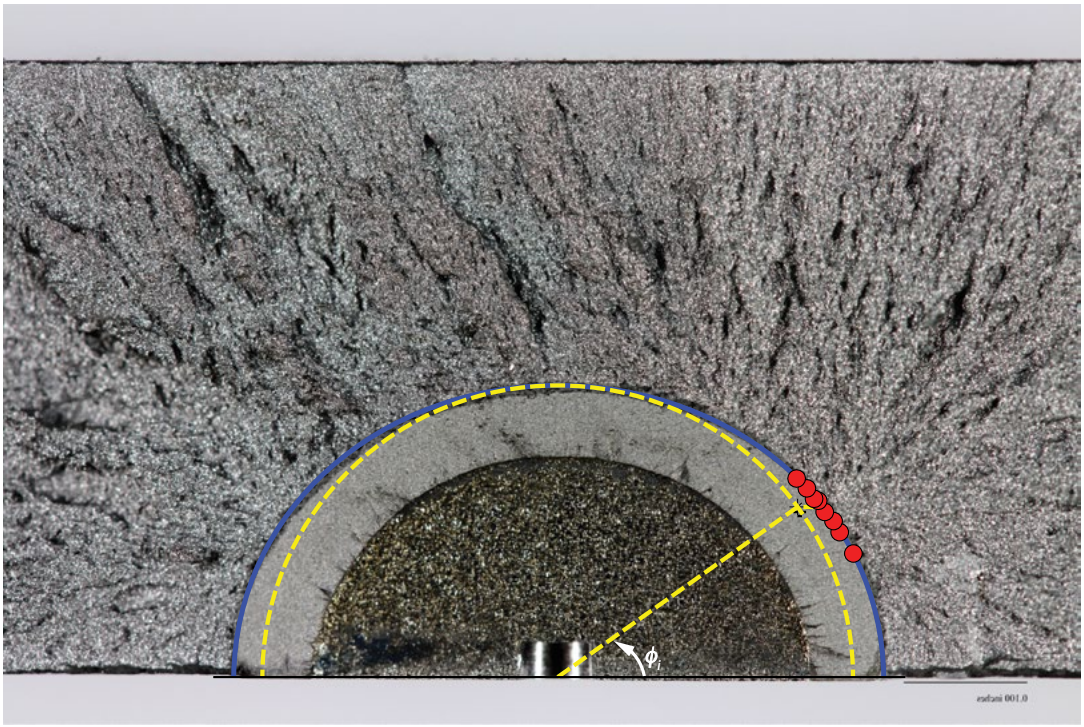

Figure 11. Illustration of the critical angle values for all ILS participants plotted on the test specimen fracture surface.

With the initiation angle established, the critical *J*-integral value (J_ϕ) corresponding to $CMOD_i$ and occurring at ϕ_i can be determined. Figure 12 shows the *J*-integral versus CMOD results at ϕ_i for all participants, and figure 13 gives a closer view of the results at CMOD equal to $CMOD_i$. In addition, the individual J_ϕ values are given in table 4. Each result set is taken at the ϕ_i location calculated by each individual participant shown in table 3a. Since the authors did not have the complete model results for each ILS participant, it was not possible to evaluate the *J*-integral versus CMOD results at a single, consensus ϕ_i value. Even so, the *J*-integral versus CMOD results are in excellent agreement for all of the analyses with <2.5% standard deviation from the average J_ϕ result. In addition, all of the J_ϕ results are within 5% of the average J_ϕ.

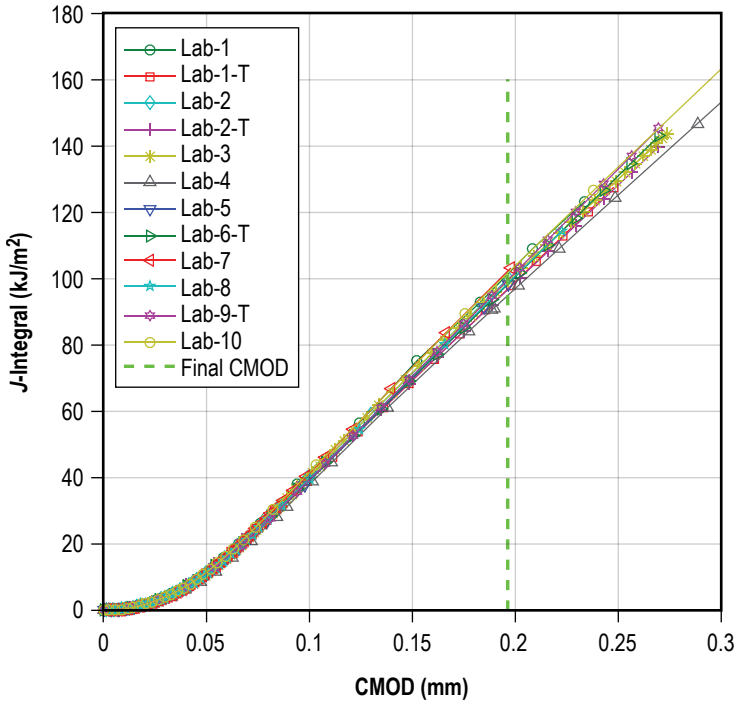

Figure 12. *J*-integral versus CMOD.

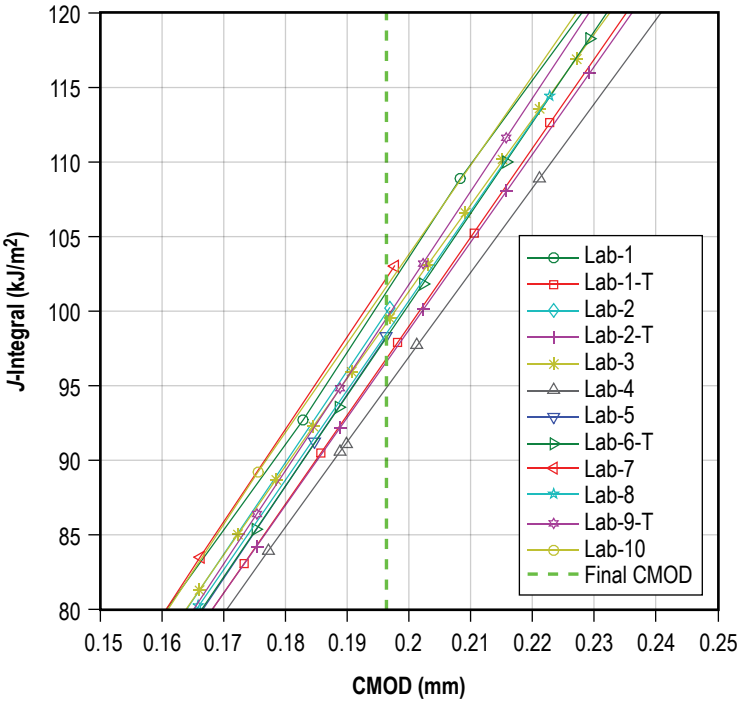

Figure 13. Closer view of the range of *J*-integral values at the critical CMOD.

Table 4. Summary of J-integral values at CMOD_i.

Lab	J (kJ/m^2) at ϕ_i
Lab-1	101.19
Lab-1-T	96.80
Lab-2	100.17
Lab-2-T	96.67
Lab-3	99.50
Lab-4	94.31
Lab-5	98.10
Lab-6-T	98.04
Lab-7	102.97
Lab-8	98.52
Lab-9-T	99.49
Lab-10	100.17

Max.	102.97
Avg.	98.83
Min.	94.31
Std. Dev.	2.29

The final step in the elastic-plastic fracture mechanics analysis of the test is the assessment of the deformation regime to determine if the J_ϕ results are valid per the deformation validity criteria in E2899 by evaluating the specimen characteristic lengths, $r_{\phi a}$ and $r_{\phi b}$ against their respective elastic-plastic regime limits. Both evaluations must be true to report a valid result in the elastic-plastic regime. First, the amount of crack-tip opening displacement must be a small fraction of the crack size such that $r_{\phi a} \geq C_{Ja}(J_\phi/\sigma_{ys})$ where

$$C_{Ja} = 15. \tag{4}$$

Second, the remaining ligament must have a sufficient size relative to the deformation such that $r_{\phi b} \geq C_{Jb}(J_\phi/\sigma_{ys})$ where

$$C_{Jb} = \frac{1}{20}\frac{E}{\sigma_{ys}} + 50\,. \tag{5}$$

All of the participants correctly reported that the J_ϕ results of this test are valid elastic-plastic regime results.

Though not necessary to perform the assessment, a graphical representation of the deformation regime and limits is shown in the Lab-1 TASC-generated plot in figure 14 to provide better insight into the deformation level relative to the E2899 EPFM limits. Figure 14 is analogous to figure 8 in E2899-13 (given as fig. 15 in this TM) wherein the vertical axis is the inverse of the deformation level ($1/C_J$) to have an increasing deformation plot in an increasing sense and the horizontal axis is the normalized crack front constraint, here T-stress/σ_{ys}. In figure 14 the blue and red curves represent the deformation trajectories for $r_{\phi a}$ (crack depth) and $r_{\phi b}$ (remaining ligament), respectively, at the calculated critical angle of $\phi_i = 36°$ while the gray curves comparatively show the same assessment for $\phi = 90°$. The deformation trajectories start at (0,0) and proceed upward and to the left as negative T-stress and J increase with increasing deformation. The green stars represent the

point of unstable fracture in the test at CMOD = CMOD$_i$. The inverse of the deformation limits for LEFM ($1/C_K$), EPFM remaining ligament ($1/C_{Jb}$), and EPFM crack depth ($1/C_{Ja}$) are plotted as black, red, and blue horizontal lines, respectively. For an assessment to be within the validity limits, the assessment point for the analysis must fall on or below its respective deformation limit line. The assessment points for this test are clearly above the LEFM limit, but both the remaining ligament and crack depth assessment points are well below their respective EPFM limits, illustrating the validity of the J_ϕ values per E2899.

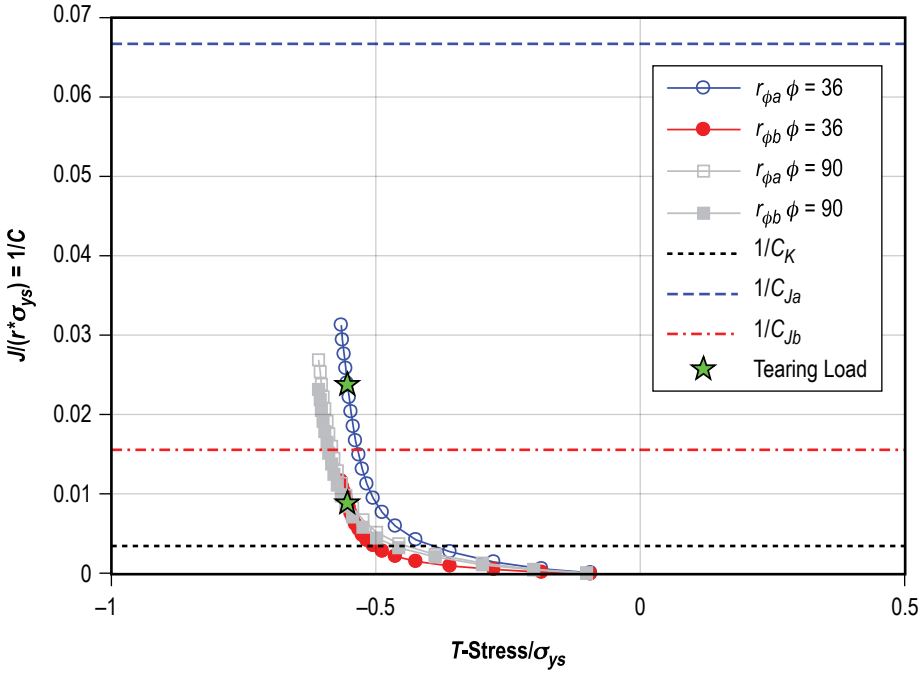

Figure 14. Lab-1 TASC assessment of crack front deformation conditions.

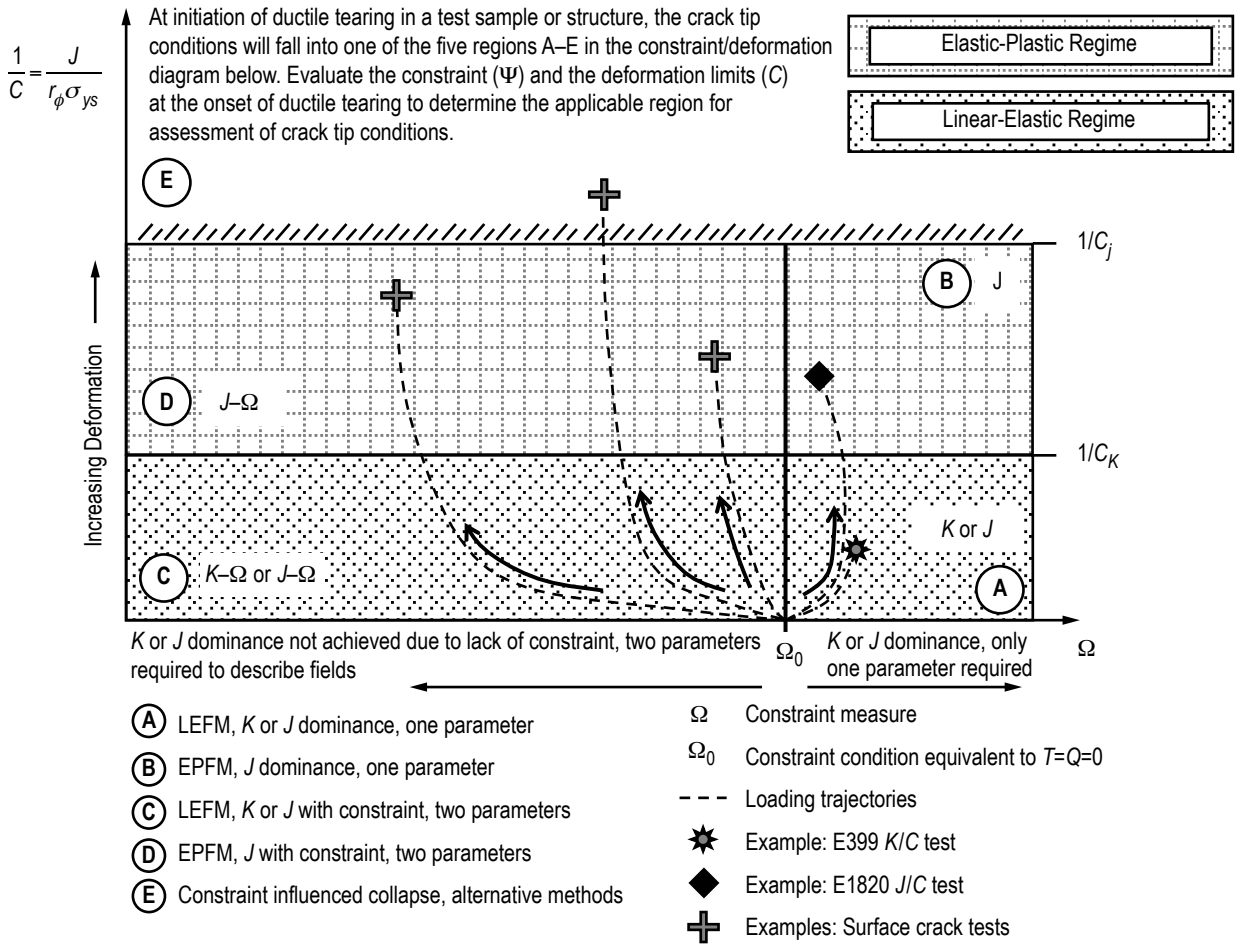

Figure 15. Figure 8 from ASTM E2899 illustrating the crack front deformation conditions and test regime assessment.

4.3 Comparison of Finite Element Modeling and the Tool for Analysis of Surface Cracks Results

In addition to the primary focus of phase II of the ILS, there was high interest in evaluating a potential new means of analysis of surface crack experiments suitable to E2899 by using interpolated solutions and the TASC software tool. The advance of surface crack fracture testing is hindered significantly by the lack of a readily available set of solutions to correlate the applied force and observed CMOD in a surface crack experiment to an evaluation of the elastic-plastic *J*-integral or deformation state of a test specimen at fracture. As reflected by the necessity for this ILS, the only practical way to fully analyze such a test is through the use of elastic-plastic FEA. A convenient and practical set of elastic-plastic surface crack solutions could help mitigate many of these obstacles; however, to date, it has proven impractical to reduce the 3D elastic-plastic surface crack solution to a set of equations suitable for inclusion in a testing standard.

To address this issue, the authors developed the computer program TASC with a graphical user interface that allows easy access to a comprehensive space of nonlinear *J*-integral solutions

for surface cracks in tension. TASC employs a methodology for interpolating between the geometric and material property variables that allows the user to estimate the *J*-integral solution around the surface crack perimeter (ϕ) as a function of loading condition from the linear-elastic regime continuously through the fully elastic-plastic regime. In addition to the *J*-integral solution, the complete force versus CMOD record is estimated to provide a direct anchor to the experimental result. The user of this interpolated solution space need only know the crack and plate geometry and the basic material flow properties to reliably evaluate the full surface crack *J*-integral and force versus CMOD solution. Thus, a solution can be obtained very rapidly by users without elastic-plastic fracture mechanics FEM experience.

Four ILS participants chose to use TASC to evaluate the test result—two were experienced analysts that used TASC in addition to their nonlinear FEA assessment (Lab-1 and Lab-2) while two other participants had limited surface crack fracture test analysis experience (Lab-6 and Lab-9) and used only TASC. In addition, Lab-9 used TASC's default material stress-strain curve fits to the provided data for the nonlinear material property inputs in the analysis without realizing that it is acceptable and desirable to adjust the default curve fit values to better fit the actual stress-strain response if needed. Even so, the TASC assessment results are clearly in family with the nonlinear FEA results. Comparing both the ϕ_i and J_ϕ values from the FEA and TASC assessments shows that the average results are within 2%, illustrating that the TASC assessments provide an answer of equivalent quality to that expected from a custom finite element assessment of the test.

5. PARTICIPANT COMMENTS

The participant comments from phase II of the ILS were encouraging. In general, the participants were able to follow the text of E2899 and work through the assessment without issues, obtaining results with little variation. Some typographical errors and confusing language were pointed out by participants which resulted in a number of changes in the E2899-15 version of the standard. By far the most common technical difficulty was in matching the initial elastic slope of the analysis and test record to the E2889-13 imposed slope matching limit of ±2.5%. As mentioned earlier, after studying the results of this ILS it was determined that an elastic slope matching the requirement of ±5% was a more reasonable metric to meet the intent of the elastic compliance check, which is reflected in the E2899-15 release.

6. CONCLUSIONS

Phase II of the ILS was fully successful with encouraging results. Ten participants with a wide range of experience volunteered to analyze a nonlinear surface crack test result following the guidance in E2899-13. The guidance on performing elastic-plastic FEA developed from phase I of the ILS and incorporated into E2899-13 provided sufficient instruction, allowing the participants to independently perform custom elastic-plastic FEA of the test. The final J_ϕ test results were in close agreement, certainly well within expected errors in other nonlinear fracture toughness test methods. In addition, participants that chose to use TASC to perform the analysis achieved results equivalent to those performing the custom FEA. Participant comments from phase II were evaluated and incorporated into changes in the E2899-15 release, resulting in an improved test standard.

APPENDIX A—PHASE II PROBLEM STATEMENT

ASTM Committee on Fatigue and Fracture
E08.07.03 Task Group on Surface Cracks

Analytical Round Robin on Elastic-Plastic Analysis of Surface Cracks in Flat Plates – Phase II

Introduction: The E08.07.03 task group published ASTM E2899 - *Standard Test Method for Initiation Toughness in Surface Cracks Under Tension and Bending* in October of 2013. This standard enables fracture toughness testing in linear-elastic and elastic-plastic regimes. In Phase I of this round robin, participants were asked to evaluate a surface crack in tension using finite element analysis. Those results can be found in NASA-TM-2012-217456, which can be retrieved from the NASA Technical Reports Server at http://ntrs.nasa.gov. In this second phase, participants are requested to evaluate a surface crack test according to the published standard. This round robin exercise is conducted under the auspices of ASTM Inter-laboratory Study 732 (ILS-732).

Objectives: 1) Determine the consistency in the interpretation of the test evaluation requirements in E2899. 2) Provide additional information on the analytical consistency of finite element (FE) methods as prescribed in the standard for future revision of the precision and bias statements. An evaluation of interpolated solutions as an alternative to FE will also be requested through use of the recently developed TASC software (Tool for Analysis of Surface Cracks).

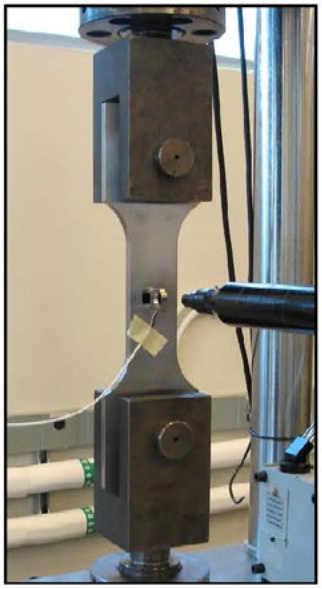

Figure 1. Experimental test.

Requested Analysis: Interpret the provided experimental data from the surface crack test shown in Figure 1 in accordance with ASTM E2899, including the test result in K or J at the critical angle ϕ_i, constraint quantification in terms of T-stress, and interpretation of selected validity criteria. Spreadsheets for recording analysis results are provided to enhance consistency in reporting and to clarify what data are being requested.

Provided Data: A compressed archive file containing the following data will be provided to each participant: instructions, material identification and stress strain data, force versus CMOD record, and the fracture surface photo (Figure 2) with basic crack size measurements. These data are intended to represent the fundamental information that would be provided by a mechanical test laboratory prior to evaluating the test result.

Figure 2. Specimen Fracture Surface - All required dimensions are provided as an annotated figure in the electronic data package. See Figure 3 for complete specimen geometry.

To Participate or Ask Questions:
Please email us:
Douglas.N.Wells@nasa.gov
Phillip.A.Allen@nasa.gov

Requested Schedule: We request that results of this Phase II assessment be returned by email (see "Questions?" box on other side) by February 15, 2014. As always, earlier would be very helpful. This will allow tabulation of the results for review at the May 2014 E08 committee meetings.

THANK YOU for participating in this very helpful study! Doug Wells and Phillip Allen, NASA MSFC.

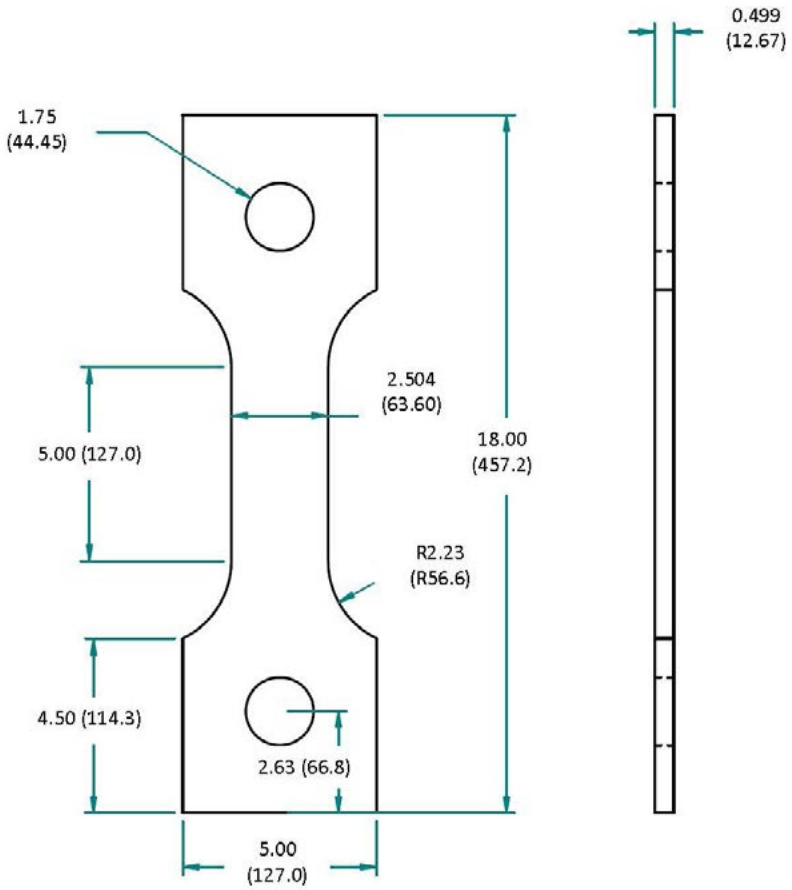

Figure 3. Specimen dimensions in inches (mm).

E08.07.03 Analytical Round Robin, Phase II – Precrack Measurements

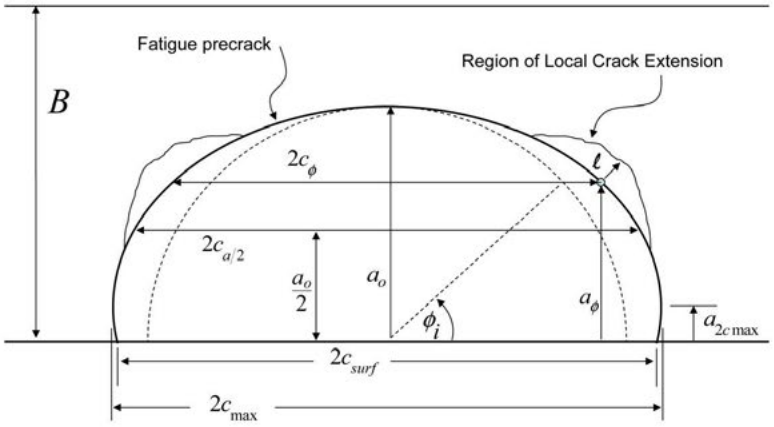

	inches (mm)
$2c_{surf}$ =	0.509 (12.93)
$2c_{max}$ =	0.516 (13.11)
$2c_{a/2}$ =	0.451 (11.46)
a_o =	0.231 (5.87)
a_{2cmax} =	0.030 (0.76)
B =	0.499 (12.67)

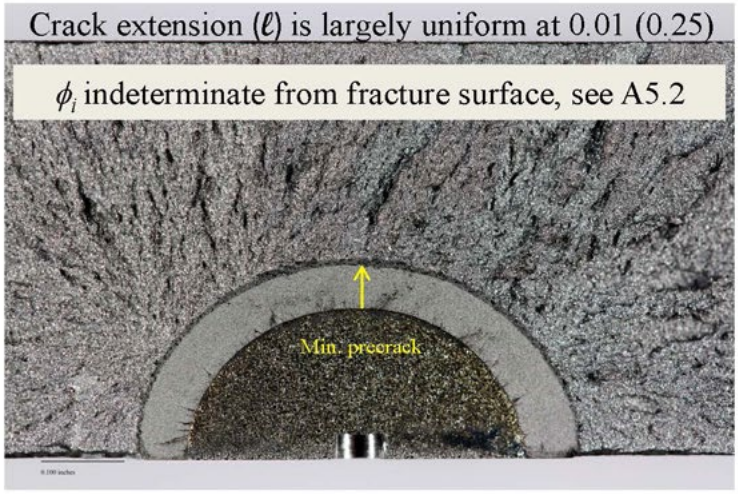

Figure 6, Precrack Extension
Min. Precrack = 0.051 (1.30)
N = 0.017 (0.43)

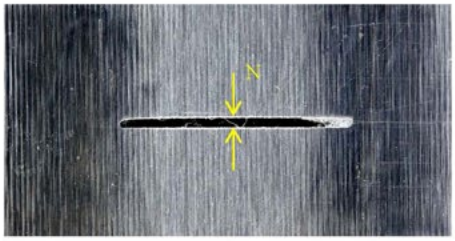

APPENDIX B—ESTIMATION OF THE CRACK EXTENSION INITIATION ANGLE FOR SURFACE CRACKS WHEN NOT DISCERNIBLE FROM THE FRACTURE SURFACE

B.1 Technical Background

With the exception of E2899[1], all of the current ASTM fracture testing standards such as E399[19] and E1820[20] take the 3D reality of the fracture toughness test and, through the use of various assumptions, simplify the problem to a 2D planar form to report an average fracture toughness representing the entire crack front. For surface crack fracture, the crack driving force is a strong function of the local crack front location, which prevents simplifying the problem into a single 2D value. Instead, the result of the surface crack fracture test is strongly dependent on being able to identify the local crack front parametric angle, ϕ. E2899 relies on post-test visual examination of the fracture surface to reveal the location of the initiation of crack tearing along the perimeter of the crack. This is generally successful for most cases when stable ductile crack extension takes place. The location of maximum tearing is assumed to be the site where crack extension began and is identified by the parametric angle, ϕ_i. Figure 16 illustrates this method as described in more detail in Annex A5 of E2899.

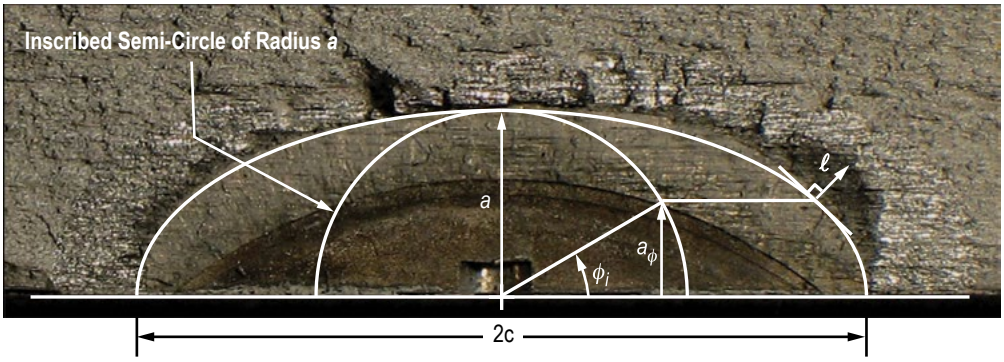

Figure 16. Definition of ϕ_i and the characterization of location of maximum crack tearing.

In some cases, the visual fractographic evidence is limited with regard to identifying the initiation location. In the case of immediate unstable ductile fracture, i.e., fracture that occurs in a 'brittle' fashion due to a flat *R*-curve shape supporting no stable crack tearing, the fracture surface may not readily reveal any clear evidence of the initiation site, short of an advanced fractographic investigation, which is outside the scope of E2899. There are also occasional cases where stable ductile tearing occurs in a sufficiently uniform manner around a large portion of the crack perimeter that a clear selection of the initiation angle is not feasible. In these cases, it is desirable to have a standardized method to establish the initiation angle, ϕ_i, to allow a test result to be generated; otherwise, the test would be considered invalid and a useful result would be discarded.

For fracture toughness evaluations in the elastic-plastic fracture mechanics regime, the *J*-integral is evaluated using elastic-plastic finite element methods to incorporate the shifts in the *J* distribution due to plasticity. However, in most cases, initiation under uniform tension stress does not occur at the maximum value of the *J*-integral along the crack perimeter, J_p, location. This strongly suggests that the crack front constraint conditions are influencing the angle of initiation. There have been many previous efforts to develop predictive methods for surface crack initiation using a crack front field amplitude parameter (*K* or *J*) combined in some fashion with a constraint parameter. Of particular interest to us is the work of Newman, Reuter, and others as described in references 15 and 16. The approach used in these studies was to apply a multiplicative factor to the local crack front field amplitude based on the local prevailing constraint conditions. Newman et al. characterized the local constraint using α_h, a constraint parameter based on the average opening mode stress over the plastic zone along a ray normal to the local crack front, normalized by the yield strength, σ_{ys}.[15,17,18] The approach has been to evaluate the parameter $K \bullet \alpha_h$ or $J \bullet \alpha_h$ along the surface crack perimeter, with the location of maximum value of the product indicating the angle of initiation. The latter method shows significant improvements to the prediction of ϕ_i compared to using only the location of J_p.

Based on these observations, for cases when the fracture surface cannot readily reveal the location of initial crack extension, a decision was made to incorporate some of this logic into E2899 to improve the estimation of ϕ_i. For simplicity purposes, the test standard uses the linear-elastic *T*-stress as the descriptor of crack front constraint as a function of ϕ, T_ϕ. Values of T_ϕ are tabulated in the standard for the requisite range of crack shapes and sizes. Given that this information is currently available and utilized in the standard, the motivation is to employ T_ϕ in a similar predictive framework as discussed above, i.e., providing a multiplicative influence factor for *J* such that their product estimates the crack perimeter location where driving force and constraint combine to provide the highest likelihood for crack extension.

The ratio of T/σ_{ys} is a good first-order estimate of the local crack front constraint condition and is capable of predicting the constraint-induced variations in crack tip opening mode stress (σ_{yy}) for surface cracks under elastic-plastic conditions.[21,22] Though σ_{yy} is likely not the sole influence factor for constraint effects in ductile fracture, the usefulness of σ_{yy} demonstrated through α_h indicates that T/σ_{ys} should be capable of providing a suitable influence factor. The ratio T/σ_{ys} can easily be related to σ_{yy} through correlation with the parameter *Q*, which represents the difference between the constraint-influenced opening mode stress and a reference stress field, typically defined at $T = 0$, evaluated at a fixed distance in front of the crack tip at $r\sigma_{ys}/J = 2$, where *r* is the radial distance from the crack tip.[23] Figure 17 illustrates the calculation of *Q* as a function of T/σ_{ys} over a range of strain-hardening coefficients, *n* for a material with an elastic modulus, *E*, to σ_{ys} ratio of 400. Note that $Q(\phi)$ is defined as a difference in σ_{yy} for the surface crack compared to σ_{yy} in the $T = 0$ reference field, therefore, $Q = 0$ when $T = 0$. To adopt the value of *Q* as an influence factor and useful multiplicative factor for *J*, the value of $Q + 1$ is chosen such that, at the neutral $T = 0$ constraint state, the multiplicative factor on *J* is unity. Lower constraint values ($T/\sigma_{ys} < 0$) provide an influence factor <1, and positive constraint conditions present an influence factor >1. From figure 17 it is clear that, for $T < 0$, the relation $T/\sigma_{ys} + 1$ is an acceptable approximation of $Q + 1$. For $T > 0$, $T/4\sigma_{ys} + 1$ provides a representation of the more subtle effects of positive *T*-stress on σ_{yy}.

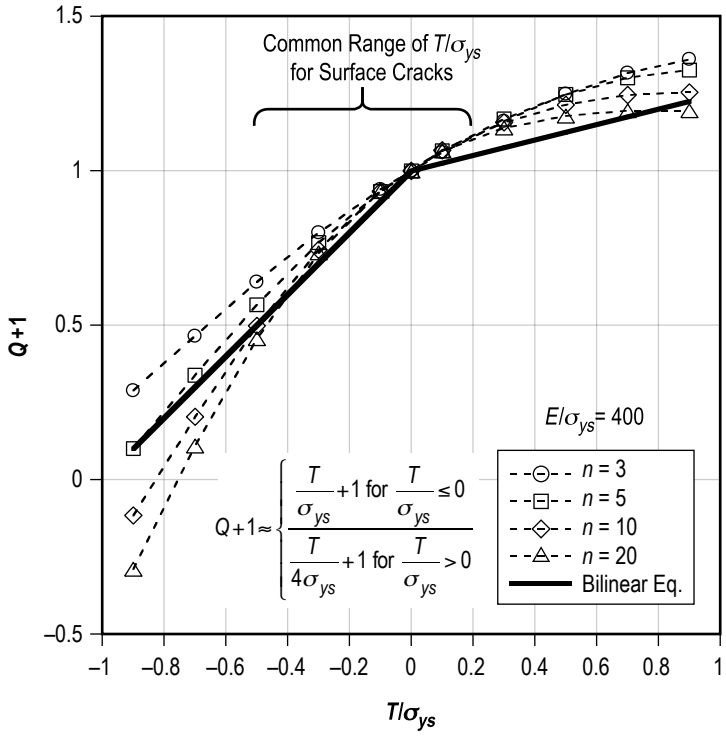

Figure 17. Relationship between T/σ_{ys} and Q.

The bilinear equation (6), provided in Annex A5 of E2899, represents a function of ϕ whose maximum identifies the estimated value for ϕ_i:

$$f(\phi) = \frac{J_\phi}{J_p}\left(\frac{T}{\sigma_{ys}}+1\right) \text{ for } \frac{T}{\sigma_{ys}} \le 0$$

$$f(\phi) = \frac{J_\phi}{J_p}\left(\frac{T}{4\sigma_{ys}}+1\right) \text{ for } \frac{T}{\sigma_{ys}} > 0\,. \tag{6}$$

Given that T/σ_{ys} is a linear-elastic concept, its values are confined to the range $-1 \le T/\sigma_{ys} \le 1$; therefore, the range of the multiplicative influence factor is from 0 to 1.25, with 1 corresponding to the $T = 0$ case and having neutral influence.

In equation (6), J_ϕ is normalized by J_p. Clearly, including J_p does not affect finding the maximum of $f(\phi)$ but this normalization renders $f(\phi)$ dimensionless and helps minimize the likelihood of it being misconstrued as a value with physical meaning.

Figure 9 illustrates the a ϕ estimation scheme based on the J_p location along with the currently proposed approach of finding ϕ_i by maximizing equation (6).

B.2 Experimental Evaluations

A common situation where experimental results indict evaluation at ϕ_i based on the J_p location occur for surface cracks in tension with half crack surface length, c, greater than the surface crack depth, a, ($c > a$) when the J_p location is often at $\phi = 90°$. In these cases, surface crack extension typically initiates closer to $15° < \phi < 35°$. A small series of 2219-T8 surface crack tests are illustrated in figure 18. All tests are tension loading except specimen 2005-B1, which was tested in four-point bending. The dashed line represents perfect agreement between measured and predicted ϕ_i. Equation (6) (open symbols) improves upon the prediction based on J_p (filled symbols).

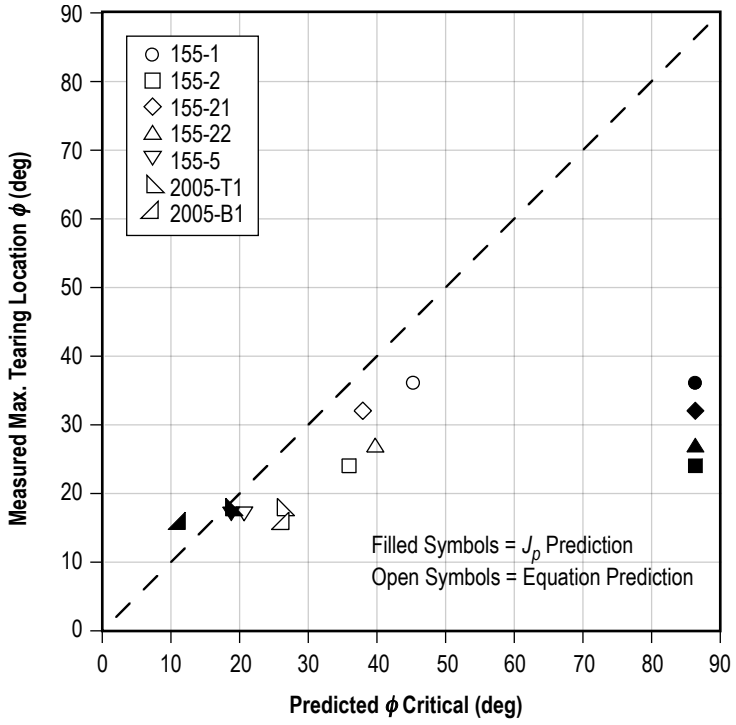

Figure 18. Performance of ϕ_i prediction based on location of J_p versus equation (6).

To further investigate the efficacy of equation (6), a number of the surface crack test data from reference 16 were reevaluated based on available data. The test specimens are D6AC steel with high strength and very little strain hardening. Figure 19 shows the results of the bend tests from the series. The use of equation (6) provides a modest improvement for a number of the tests. Others are just as closely predicted by the J_p location. A larger collection of reliable bend tests with known ϕ_i is needed. After further study, it may prove sufficient to use the J_p location to estimate ϕ_i for bend tests in lieu of the effort required to find the maximum of equation (6). Currently, E2899 requires using equation (6) for all tests that do not reveal ϕ_i in the fracture surface morphology.

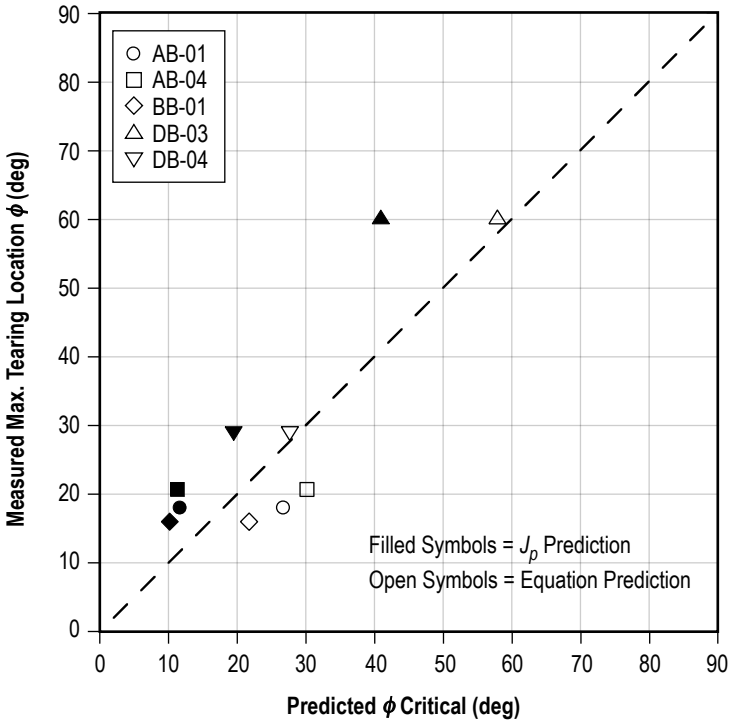

Figure 19. Performance of ϕ_i prediction for D6AC bend tests.

Figures 20 and 21 show the results for the estimation of ϕ_i in the tension tests from the D6AC study. In this case, the results for J_p and equation (6) are shown in separate figures for better clarity. Again, the most striking improvement comes in the prediction of tension tests where J_p occurs at the crack depth. The constraint distribution moves the location of the initial crack extension toward $15° < \phi < 35°$, and equation (6) generally predicts this well.

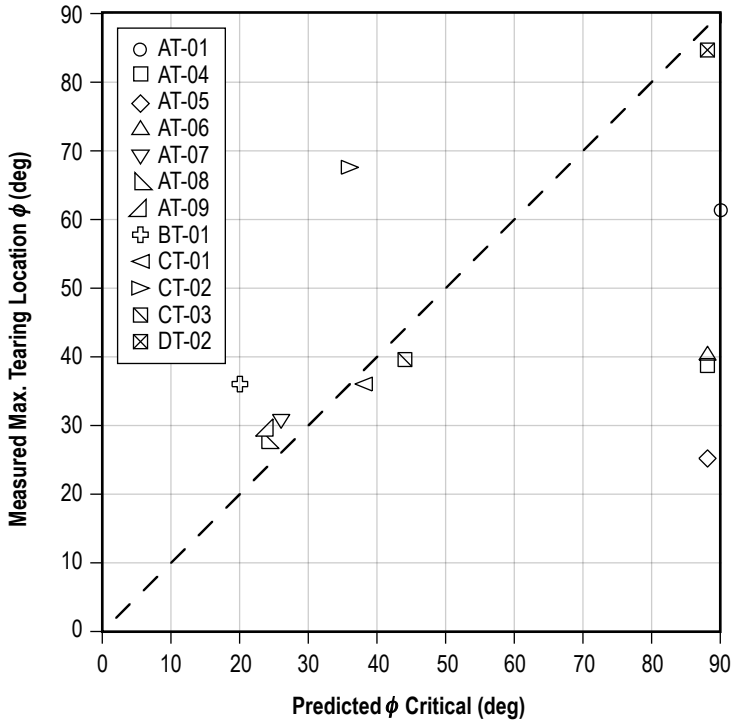

Figure 20. Predicted ϕ_i based on J_p for D6AC tension specimens.

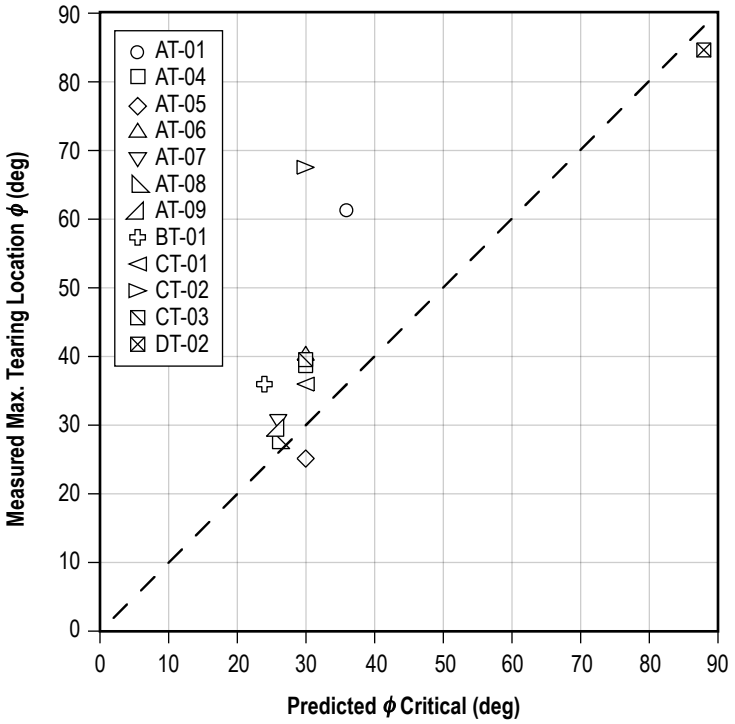

Figure 21. Predicted ϕ_i based on equation (6) for D6AC tension specimens.

Figure 21 also illustrates that this predictive methodology remains an estimation that cannot account for all possibilities (CT-02) and there are clearly some weaknesses that may be addressed with further study:

- Different materials exhibit a range of sensitivity to constraint due to the particulars of their micromechanical fracture process. The influence coefficient based on opening mode stress should likely vary with the constraint sensitivity of the material.

- The opening mode stress model may not always be the best parameter to base the influence coefficient on. Other parameters, such as the Rice and Tracey ductile void growth model[24] correlated to T/σ_{ys} may prove beneficial for some materials.

- Typical material variability, local material defects near the crack front, as well as toughness anisotropy can strongly affect ϕ_i. These effects are absent from this methodology.

- For tests with high deformation, approaching the end of the defined elastic-plastic regime in the standard, the linear-elastic T-stress concept becomes an increasing suspect and may not accurately reflect the true magnitude and distribution of constraint conditions around the crack perimeter.

Frequently, the strong variability inherent to determining ϕ_i, whether directly from interpreting the fracture surface (which is often not as easy as one would hope) or from estimating ϕ_i using methods such as equation (6), is not nearly as prevalent in the calculated value of the test result (J_ϕ), because the most common cause for ambiguity in ϕ_i is a nominally uniform distribution of J and constraint around the crack. In these cases, the J_ϕ result is fairly insensitive to ϕ_i.

B.3 Conclusion

The proposed use of equation (6) is only for cases where the fracture surface refuses to yield the value of ϕ_i. In these cases, rather than reject an expensive test result, it is worthwhile to have a reasonable engineering estimate of ϕ_i for evaluating the test. The preponderance of experimental evidence suggests that using the ϕ location corresponding to J_p is frequently inaccurate, particularly for tests in uniaxial tension. The previous work of Newman et al. provides a substantial foundation on which to reformulate the model based on the T/σ_{ys} constraint parameter already available as part of the test standard. Though not a universal panacea, the use of equation (6) generally represents a significant improvement over just using J_p in cases where ϕ_i must be estimated.

REFERENCES

1. ASTM E2899-15, Standard Test Method for Measurement of Initiation Toughness in Surface Cracks Under Tension and Bending, <http://www.astm.org/Standards/E2899.htm> (verified March 18, 2016).

2. Newman, Jr., J.C.; and Raju, I.S.: Stress-Intensity Factor Equations for Cracks in Three-Dimensional Finite Bodies Subjected to Tension and Bending Loads, *Computational Methods in the Mechanics of Fracture*, Vol. 2, pp. 311–334, 1986.

3. Newman, Jr., J.C.; Reuter, W.G.; and Aveline, C.R.: Stress and Fracture Analyses of Semi-Elliptical Surface Cracks, ASTM Special Technical Publication, STP1360: pp. 403–423, doi: 10.1520/STP13417S, 2000.

4. API A, API 579-1/ASME FFS-1, *Fitness-For-Service, Second Edition*, American Petroleum Institute, 2007.

5. ASTM E1820-15, Standard Test Method for Measurement of Fracture Toughness, <http://www.astm.org/Standards/E1820.htm> (verified March 18, 2016).

6. Wells, D.N.; and Allen, P.A.: "Analytical Round Robin for Elastic-Plastic Analysis of Surface Cracked Plates: Phase I Results," NASA/TM—2012–217456, NASA Marshall Space Flight Center, Huntsville, AL, 94 pp., March 2012.

7. Bleackley, M.H.; and Luxmoore, A.R.: "Comparison of finite element solutions with analytical and experimental data for elastic-plastic cracked problems," *International Journal of Fracture*, Vol. 22, No. 1, pp. 15–39, doi: 10.1007/BF00960097, May 1983.

8. Larrson, L.H.: "A calculational round robin in elastic-plastic fracture mechanics," *International Journal of Pressure Vessels and Piping*, Vol. 11, No. 4, pp. 207–228, doi.org/10.1016/0308-0161(83)90042-X, April 1983.

9. Allen, P.A.; and Wells, D.N.: "Elastic-Plastic *J*-Integral Solutions for Surface Cracks in Tension Using an Interpolation Methodology," NASA/TM—2013–217480, NASA Marshall Space Flight Center, Huntsville, AL, 104 pp., April 2013.

10. Allen, P.A.; and Wells, D.N.: "Interpolation methodology for elastic-plastic *J*-integral solutions for surface cracked plates in tension," *Engineering Fracture Mechanics*, Vol. 119, pp. 173–201, doi.org/10.1016/j.engfracmech.2014.02.021, March 2014.

11. Allen, P.A.: Tool for Analysis of Surface Cracks (TASC), TASC NASA, <https://source-forge.net/projects/tascnasa/> (verified March 18, 2016).

12. Graham, S.M.; and Adler, M.A.: "Determining the Slope and Quality of Fit for the Linear Part of a Test Record," *Journal of Testing and Evaluation*, Vol. 39, No. 2, pp. 260–268, doi.org/10.1520/JTE103038, March 2011.

13. Anderson, T.L.: *Fracture Mechanics: Fundamentals and Applications*, 3rd ed., CRC Press, 2005.

14. Brocks, W.; and Scheider, I.: "Reliable J-Values—Numerical aspects of the path-dependence of the J-integral in incremental plasticity," *MP Materialprüfung*, Vol. 45, No. 6, p. 264, January 2003.

15. Newman, Jr., J.C.; Reuter, W.G.; and Aveline, C.R.: "Stress and Fracture Analyses of Semi-Elliptical Surface Cracks," ASTM STP 1360, pp. 403–423, 1999.

16. Leach, A.M.; Daniewicz, S.R.; and Newman, Jr., J.C.: "A new constraint based fracture criterion for surface cracks, *Engineering Fracture Mechanics*, Vol. 74, No. 8, pp. 1233–1242, May 2007.

17. Aveline, Jr., C.R.; and Daniewicz, S.R.: "Variations of Constraint and Plastic Zone Size in Surface-Cracked Plates Under Tension or Bending Loads," ASTM STP 1389, pp. 206–220, doi: 10.1520/STP14802S, January 2000.

18. Newman, Jr., J.C.; Bigelow, C.A.; and Shivakumar, K.N.: "Three-dimensional elastic-plastic finite-element analyses of constraint variations in cracked bodies," *Engineering Fracture Mechanics*, Vol. 46, No. 1, pp. 1–13, September 1993.

19. ASTM E399-12, Standard Test Method for Linear-Elastic Plane-Strain Fracture Toughness K_{Ic} of Metallic Materials, <http://www.astm.org/Standards/E399.htm> (verified March 18, 2016).

20. ASTM E1820-15, Standard Test Method for Measurement of Fracture Toughness, <http://www.astm.org/Standards/E1820.htm> (verified March 18, 2016).

21. Wang, Y.: On the Two-Parameter Characterization of Elastic-Plastic Crack-Front Fields in Surface-Cracked Plates, ASTM International, STP1171, pp. 120–138, January 1993.

22. Wang, Y.; and Parks, D.M.: "Limits of J-T characterization of elastic-plastic crack-tip fields," *Constraints in Fracture Theory and Applications*: *Second Volume*, ASTM STP 1244, American Society for Testing and Materials, Philadelphia, pp. 43–67, 1995.

23. O'Dowd, N.P.; and Shih, C.F.: "Family of crack-tip fields characterized by a triaxiality parameter—I. Structure of fields," *Journal of Mechanics and Physics of Solids*, Vol. 39, No. 8, pp. 989–1015, December 1991.

24. Rice, J.R.; and Tracey, D.M.: "On the Ductile Enlargement of Voids in Triaxial Stress Fields," *Journal of Mechanics and Physics of Solids*, Vol. 17, No. 3, pp. 201–217, 1969.

REPORT DOCUMENTATION PAGE

Form Approved
OMB No. 0704-0188

1. REPORT DATE *(DD-MM-YYYY)*	2. REPORT TYPE	3. DATES COVERED *(From - To)*
01–03–2017	Technical Memorandum	

4. TITLE AND SUBTITLE

Analytical Round Robin for Elastic-Plastic Analysis of Surface Cracked Plates, Phase II Results

5a. CONTRACT NUMBER

5b. GRANT NUMBER

5c. PROGRAM ELEMENT NUMBER

6. AUTHOR(S)

P.A. Allen and D.N. Wells

5d. PROJECT NUMBER

5e. TASK NUMBER

5f. WORK UNIT NUMBER

7. PERFORMING ORGANIZATION NAME(S) AND ADDRESS(ES)

George C. Marshall Space Flight Center
Huntsville, AL 35812

8. PERFORMING ORGANIZATION REPORT NUMBER

M–1424

9. SPONSORING/MONITORING AGENCY NAME(S) AND ADDRESS(ES)

National Aeronautics and Space Administration
Washington, DC 20546–0001

10. SPONSORING/MONITOR'S ACRONYM(S)

NASA

11. SPONSORING/MONITORING REPORT NUMBER

NASA/TM—2017–218233

12. DISTRIBUTION/AVAILABILITY STATEMENT

Unclassified-Unlimited
Subject Category 39
Availability: NASA STI Information Desk (757–864–9658)

13. SUPPLEMENTARY NOTES

Prepared by the Materials and Processes Laboratory, Engineering Directorate

14. ABSTRACT

The second phase of an analytical round robin for the elastic-plastic analysis of surface cracks in flat plates was conducted under the auspices of ASTM Interlaboratory Study 732. The interlaboratory study (ILS) had 10 participants with a broad range of expertise and experience, and experimental results from a surface crack tension test in 4142 steel plate loaded well into the elastic-plastic regime provided the basis for the study. The participants were asked to evaluate a surface crack tension test according to the version of the surface crack initiation toughness testing standard published at the time of the ILS, E2899-13. Data were provided to each participant that represent the fundamental information that would be provided by a mechanical test laboratory prior to evaluating the test result. Overall, the participant's test analysis results were in good agreement and constructive feedback was received that has resulted in an improved published version of the standard E2899-15.

15. SUBJECT TERMS

surface crack, fracture toughness, *J*-integral, elastic-plastic analysis, finite element analysis, fracture toughness testing, ASTM E2899

16. SECURITY CLASSIFICATION OF:			17. LIMITATION OF ABSTRACT	18. NUMBER OF PAGES	19a. NAME OF RESPONSIBLE PERSON
a. REPORT	b. ABSTRACT	c. THIS PAGE			STI Help Desk at email: help@sti.nasa.gov
U	U	U	UU	52	19b. TELEPHONE NUMBER *(Include area code)* STI Help Desk at: 757–864–9658

National Aeronautics and
Space Administration
IS02
George C. Marshall Space Flight Center
Huntsville, Alabama 35812